


## Article

# Understanding the Luminescence Characteristics of Ultraviolet InGaN/AlGaN Multiple Quantum Wells with Different In Gradients

Jie Zhang , Wei Liu \* and Shuyuan Zhang

School of Microelectronics, Northwestern Polytechnical University (NWPUP), Xi'an 710000, China; 1754588919@mail.nwpu.edu.cn (J.Z.); zsy00@mail.nwpu.edu.cn (S.Z.)

\* Correspondence: liuweil27@nwpu.edu.cn

**Abstract:** The electroluminescence (EL) properties of InGaN/AlGaN ultraviolet light-emitting multiple quantum wells (MQWs) with identical average In content but different In gradients (In content increases linearly, along the growth direction) are investigated numerically. It is found that the luminescence efficiency is improved, and the EL spectral peak wavelength becomes longer for the MQW sample with a larger In gradient. Since the influence of In gradient is different for the conduction and valence bands in InGaN layers, the distribution of electrons and holes in QWs may be changed, leading to a redshift of EL spectra. In particular, when the In gradient increases, the overlap integral of electron-hole wavefunction in InGaN QWs increases, resulting in a higher radiative recombination rate and an enhanced EL intensity.

**Keywords:** InGaN/AlGaN multiple quantum wells; In gradient; carrier distribution; wavefunction



**Citation:** Zhang, J.; Liu, W.; Zhang, S. Understanding the Luminescence Characteristics of Ultraviolet InGaN/AlGaN Multiple Quantum Wells with Different In Gradients. *Crystals* **2021**, *11*, 1390. <https://doi.org/10.3390/cryst11111390>

Academic Editor: Claudio Cazorla

Received: 15 October 2021

Accepted: 12 November 2021

Published: 15 November 2021

**Publisher's Note:** MDPI stays neutral with regard to jurisdictional claims in published maps and institutional affiliations.



**Copyright:** © 2021 by the authors. Licensee MDPI, Basel, Switzerland. This article is an open access article distributed under the terms and conditions of the Creative Commons Attribution (CC BY) license (<https://creativecommons.org/licenses/by/4.0/>).

## 1. Introduction

Group-III nitrides (AlN, GaN, and InN) and their ternary and quaternary alloy materials have attracted lots of research interest in the field of semiconductor optoelectronic materials because of the wide and tunable direct band-gap structures covering the spectral range from ultraviolet (UV) to infrared [1–3]. Currently, more research focuses on the solid-state GaN-based UV light-emitting diodes (LEDs) due to the great potential applications in ink curing, biomedicine, and water and air purification [4,5]. However, compared with the extensively used LEDs for displaying and illumination, the GaN-based UV LEDs still suffer from many scientific and technical problems. For example, for UV LEDs based on InGaN/GaN multiple quantum wells (MQWs), the In content in InGaN well layers is very small, and correspondingly, the height of the GaN potential barrier is too low to effectively restrict electrons within QWs, causing a serious leakage of electrons [6]. Therefore, AlGaIn materials with wider band gaps are generally used as quantum barriers in GaN-based UV LEDs to increase the height of potential barriers and enhance the ability to capture and confine carriers in the MQW active region, leading to a reduced leakage current, as well as an enhanced device performance of UV LEDs [7].

However, due to the strong lattice mismatch between AlGaIn and InGaIn materials, the misfit dislocations induced by lattice relaxation at the AlGaIn/InGaIn interfaces in the MQW active region may increase, resulting in the deterioration of MQW crystal quality and a reduction in luminescence efficiency [8,9]. On the other hand, for coherently grown MQW layers, the strong lattice mismatch may also generate a large number of polarization charges at the InGaIn/AlGaIn interfaces due to the piezoelectric polarization effect, which enhances the polarization-induced electric field in InGaIn QWs and leads to a stronger quantum-confined Stark effect (QCSE) [10,11]. It is well known that the luminescence efficiency of InGaIn QWs can be reduced significantly by strong QCSE [12]. Therefore, to improve the device performance, many research efforts have focused on reducing

QCSE in AlGaIn/InGaIn MQWs with large lattice mismatch by adopting optimized barrier structures, such as GaN/AlGaIn/GaN triangular or stepped composite barriers [13,14], plasma-doped high-quality GaN buffer layers [15], or lattice-matched AlInGaIn quaternary alloy barriers [16]. It was found that when the In content gradually increases along the epitaxial growth direction in InGaIn well layers, QCSE may be weakened and luminescence efficiency can be improved significantly [17–22]. However, the discussion about the related physical mechanisms is less sufficient in the literature. Therefore, to gain a deeper insight into this problem, the effects of linearly increased In content with different gradients on the luminescence properties of UV AlGaIn/InGaIn MQWs are investigated numerically in this paper. It is found that for the MQW sample with larger gradient of In content, the luminescence intensity is enhanced and the spectrum redshifts, which may be ascribed to the different variations of conduction and valence bands induced by the linear increase in In content in InGaIn QWs and will be discussed in detail later.

## 2. Sample Structure and Simulation Models

The studied UV InGaIn/AlGaIn MQW sample is composed of the following four parts: a 3  $\mu\text{m}$ -thick n-type GaN layer with doping concentration of  $2 \times 10^{18} \text{ cm}^{-3}$ , 4-periodic InGaIn/Al<sub>0.05</sub>GaN MQW active region, a 20 nm-thick p-type Al<sub>0.15</sub>GaN electron-blocking layer (EBL) with doping concentration of  $1 \times 10^{20} \text{ cm}^{-3}$ , and a 0.3  $\mu\text{m}$ -thick p-type GaN layer with doping concentration of  $1 \times 10^{20} \text{ cm}^{-3}$ . In the MQW active region, the thickness of InGaIn well and AlGaIn barrier layers are set to be 3 and 10 nm, respectively. In order to study the electroluminescence (EL) characteristics of UV MQWs, the vertical electrical injection structure is used, i.e., the anode and cathode of the PN junction are directly placed on the top of p-type GaN layer and the bottom of n-type GaN layer, respectively. The In content in InGaIn well layer increases linearly along the growth direction for all samples, but the gradients (or the increase rates) of In content are different from each other.

The In content in InGaIn well layers of sample A increases linearly from 4% to 6%, and that of sample B increases from 3% to 7%. For samples C and D, the increases of In content are from 2% to 8% and from 1% to 9%, respectively. To be clear, the conduction and valence bands of single InGaIn QW with different gradients of In content are schematically plotted in Figure 1, where the polarization electric field is ignored for simplification. For the InGaIn QWs with linearly increased In content, the average In content,  $c$ , and the gradient,  $g$ , of In content in well layers can be calculated as:

$$c = (c_H + c_L)/2 \quad (1)$$

$$g = (c_H - c_L)/w \quad (2)$$

where  $c_H$  and  $c_L$  represent the highest and lowest In contents in InGaIn QW, respectively, and  $w$  represents the QW width. The calculation shows that the average In content in InGaIn QWs of all samples are identical, at 5%. However, from samples A to D, the gradients of In content are 0.67, 1.33, 2.00, and 2.67%/nm, respectively. In short, the In gradient increases from samples A to D, although the average In content in QWs is the same for all samples.

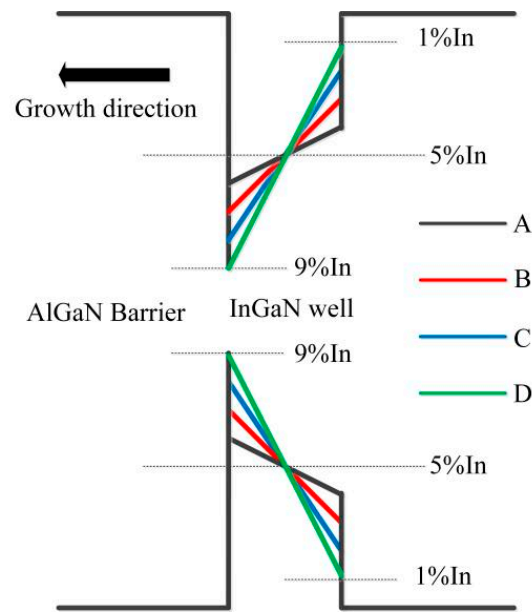


**Figure 1.** Schematic diagrams of energy bands of InGaN QW with different In gradients for samples A, B, C and D. The polarization effect is not considered here for simplification.

We theoretically studied different structures by using the Silvaco simulation program. In this study, the designed LEDs were simulated by a simulator of light emitters based on nitride semiconductors software using a three-band wurtzite k-p model. The band offset ratio, defined as the ratio between the conduction band offset and valence band offset, was set to be 7:3 for the samples [23,24]. The general radiative recombination rate is set to be  $2 \times 10^{-11} \text{ cm}^3/\text{s}$ . An Auger recombination coefficient of  $5 \times 10^{-31} \text{ cm}^6/\text{s}$  and an SRH coefficient of 100 ns are adopted in our simulation [25]. Spontaneous and piezoelectric polarization charge models were included in the simulation. The polarization charge density due to spontaneous and piezoelectric polarizations at the interface of InGaN/AlGaN is calculated by the methods developed by Fiorentini et al. [26]. The total charge density is the sum of spontaneous and piezoelectric polarization charges at the interface of different layers. In this study, we used 40% of total calculated polarization charge for InGaN and AlGaN in the simulation [27]. The coupled solution process of Poisson-Schrödinger equations, current continuity equations of electrons and holes, and carrier drift-diffusion transport equations are used in numerical solution methods [27]. The Poisson-Schrödinger equations relate the electrostatic potential to the space-charge density:

$$\text{div}(\epsilon \nabla \psi) = -\rho \quad (3)$$

where  $\Psi$  is the electrostatic potential,  $\epsilon$  is the local permittivity, and  $\rho$  is the local space-charge density. The continuity equations for electrons and holes are defined by equations:

$$\frac{\partial n}{\partial t} = \frac{1}{q} \text{div} \vec{J}_n + G_n - R_n \quad (4)$$

$$\frac{\partial p}{\partial t} = -\frac{1}{q} \text{div} \vec{J}_p + G_p - R_p \quad (5)$$

where  $n$  and  $p$  are the electron and hole concentration, respectively,  $\vec{J}_n$  and  $\vec{J}_p$  are the electron and hole current densities, respectively,  $G_n$  and  $G_p$  are the generation rates for electrons and holes, respectively,  $R_n$  and  $R_p$  are the recombination rates for electrons and

holes, respectively, and  $q$  is the magnitude of the charge on an electron. The drift-diffusion transport equations are defined by equations:

$$\vec{J}_n = qn\mu_n\vec{E}_n + qD_n\nabla n \quad (6)$$

$$\vec{J}_p = qp\mu_p\vec{E}_p - qD_p\nabla p \quad (7)$$

where  $\vec{E}_n$  and  $\vec{E}_p$  are the effective electric fields of electrons and holes, respectively,  $\mu_n$  and  $\mu_p$  are the electron and hole mobilities, respectively, and  $D_n$  and  $D_p$  are the diffusion coefficient of electrons and holes, respectively.

### 3. Results and Discussion

Figure 2 shows the numerical EL spectra of all samples simulated at a forward-injection current of 100 mA (200 A/cm<sup>2</sup>). It is found that the peak wavelengths of EL spectrum increase from samples A to D, i.e., the sample's EL spectrum redshifts with increasing In gradient. Generally, for InGa<sub>1-x</sub>N QWs, the QCSE-induced redshift of EL spectrum often accompanies a decrease in luminescence efficiency. However, it is surprising to notice that the EL spectral intensities increase with an increase in In gradient from samples A to D, as seen in Figure 2.

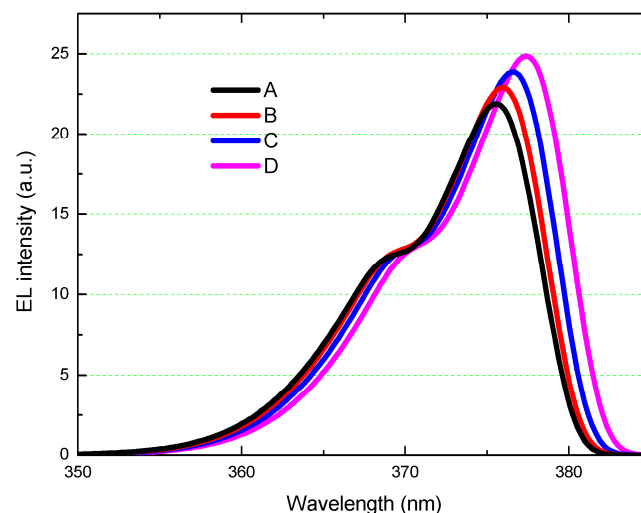


**Figure 2.** EL spectra of samples A, B, C and D under 100-mA injection current.

In order to analyze this abnormal spectral change, the calculated structures of conduction and valence bands of all samples' active regions at the forward-injection current of 100 mA are depicted in Figures 3 and 4. It is clear to see that the structures of conduction and valence bands of samples A, B, C, and D are different from each other when the gradient of In content increases. It is well known that when the In content in InGa<sub>1-x</sub>N QWs is constant, both the conduction and valence bands of InGa<sub>1-x</sub>N QWs are tilted downward along the epitaxial growth direction because of the piezoelectric polarization electric field in InGa<sub>1-x</sub>N layers [27,28]. However, in Figure 4, when the In content in InGa<sub>1-x</sub>N QW increases linearly along the growth direction, the variations of valence and conduction bands are different. For the valence bands, the tilt directions of valence bands in InGa<sub>1-x</sub>N QWs of samples A and B with small In gradient are generally downward along the growth direction, whereas the QWs' valence bands of sample C are almost flat, and those of sample D even slightly tilt upward along the growth direction. In other words, the valence band in QWs of sample D with the largest In gradient shows the opposite tilt direction compared with the small-In-gradient samples A and B. For the case of conduction bands, the tilt directions in InGa<sub>1-x</sub>N QWs are the same for all samples, i.e., they all tilt downward along the growth

direction. The only difference is that the tilt degree increases with increasing In gradient from samples A to D.

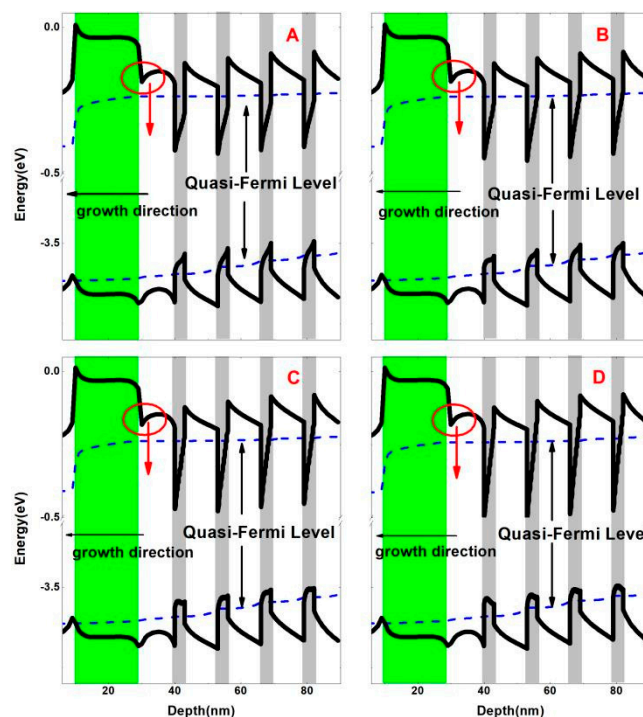


Figure 3. Energy-band structures of samples A, B, C and D.

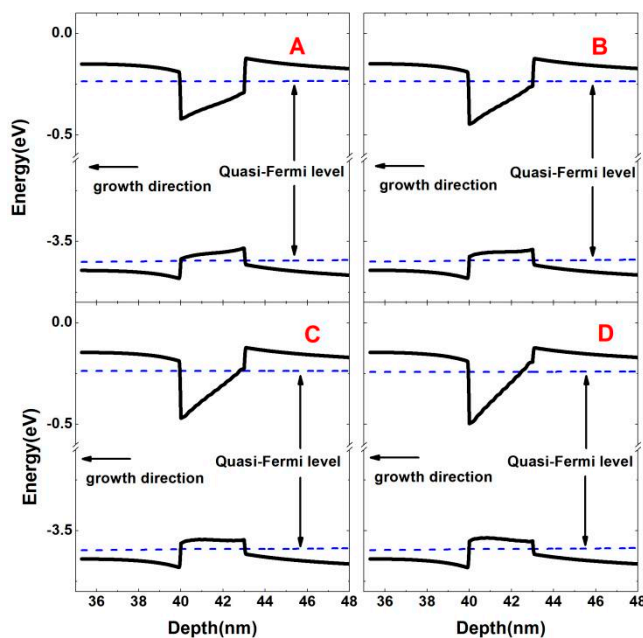
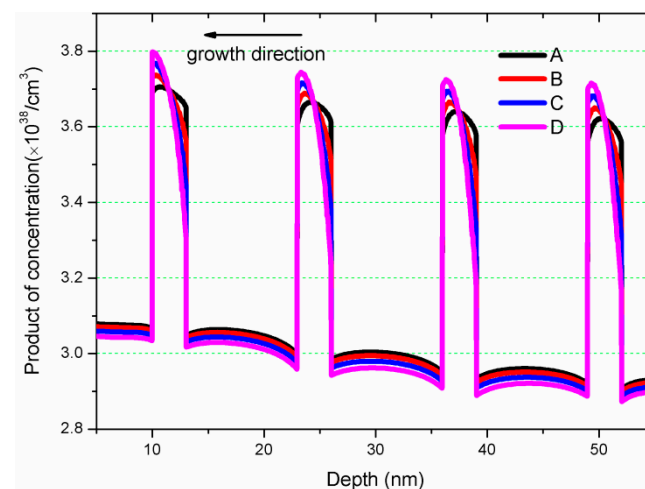


Figure 4. Energy band of the last well of samples A, B, C and D.

On the one hand, it is known that the polarization electric field can tilt the energy band in InGaN QWs downward along the growth direction. On the other hand, due to the linear increase in In content along the growth direction, the band gap in InGaN QWs gradually narrows along the growth direction. As a result, the bottom of the conduction band and the top of the valence band move toward the center of the forbidden band in QWs along the growth direction. Thus, in InGaN QWs along the growth direction, the bottom of the

conduction band is pulled down, while the top of the valence band is raised up. It turns out to be that the increase in In content in InGaN QWs can strengthen the polarization-induced tilt of the conduction band but counteract that of the valence band. Since the energy bands of InGaN QWs are jointly influenced by the polarization field and the linearly varied In content in InGaN layers, the tilt of the conduction band in InGaN QWs becomes more serious, while that of the valence band is weakened. Therefore, as shown in Figure 4, with increased In gradient from samples A to D, the conduction band tilts more seriously, while the valence band becomes less tilted. In particular, for samples C and D, with larger gradient of In content in InGaN QWs, the band gap narrows significantly along the growth direction, which may overwhelm the influence of the polarization electric field on the energy bands. As a result, the QWs' valence band of sample C is almost flattened, and that of sample D even tilts upward slightly along the growth direction. In addition, we also found that the spectrum shows shoulders around 370 nm, and the main cause may be the small quantum wells in the interface of the last quantum barrier and EBL, as shown in Figure 3.

It is considered that the changed tilt status of energy bands may impact the carrier distribution in InGaN QWs. Therefore, the concentration product of injected electrons and holes at 100mA injection current are plotted and compared in Figure 5 for all samples. Since the radiative recombination rate is proportional to the product of electron-hole concentration [29], the peak position of electron-hole concentration product corresponds to the position where the radiative recombination rate of carriers is the highest in InGaN QWs.



**Figure 5.** Comparison of electron-hole concentration product in InGaN QWs for samples A, B, C and D.

It can be seen from Figure 5 that as the In gradient increases from samples A to D, the peak position of the electron-hole concentration product approaches the left side of InGaN QWs. In fact, it can be seen from the energy band diagrams in Figure 4 that when the In gradient is small, e.g., sample A, the tilt directions of conduction and valence bands are basically the same. This means that the electrons and holes are distributed on the left and right sides of InGaN QWs, respectively, and the electron-hole concentration product is almost uniform in QWs. As the In gradient increases, the tilt of the conduction band becomes more serious, making the accumulation of electrons on the left side of InGaN QWs more significant. On the contrary, the valence band is less tilted and even becomes flat or tilts reversely with increasing In gradient, which makes more holes move from the right to the left side of InGaN QWs. Therefore, it can be seen in Figure 5 that from samples A to D, the peak position of the electron-hole concentration product gradually approaches the left side of QWs, since both the electrons and holes concentrate on the left side of InGaN QWs. In fact, because the In content increases linearly along the growth direction, the In content on the left side of InGaN QWs is the highest, which forms the region with the deepest



potential well in InGaN layers. Therefore, the peak position of electron-hole concentration product moves to the left side of QWs where the In content is the highest in the InGaN QWs, as both electrons and holes tend to fill the deep potential well. On the other hand, the values of the highest In content in QWs of samples A, B, C, and D are 6%, 7%, 8% and 9%, respectively, i.e., the highest In content increases with increased In gradient. As a consequence, the EL spectra redshift from samples A to D, as shown in Figure 2, since more carriers may concentrate on the left side of InGaN layers where the highest In content increases with increased In gradient.

To further explore the reason responsible for the variation of samples' EL intensities, the wavefunctions of electrons and holes in the last InGaN QW, which is close to the EBL, are studied and depicted at the injection current of 100 mA in Figure 6. It is seen that as the In gradient increases, the overlap of wavefunctions of electrons and holes in InGaN QWs increases. For example, the overlap ratio of wavefunctions in sample A is 66.86%, whereas that of D increases to 73.43%. In fact, from the energy-band structures in Figure 4, it is noted that for sample A, the tilt directions of conduction and valence bands are basically the same. Thus, the electrons and holes mainly distribute on the left and right sides of InGaN QWs, respectively, leading to a small wavefunction overlap ratio. As the In gradient increases for samples C and D, the tilt of the conduction band is promoted, while the valence band becomes flattened or even reversely tilted. Since the effective mass of electrons is very small, the distribution of electron wavefunction in QWs is less impacted by the promoted tilt of the conduction band. However, the distribution of holes may be affected significantly by the varied valence band, for the effective mass of hole is much larger than that of electron. Therefore, the hole wavefunction may move toward the left side of QWs due to the flattened and even reversely tilted valence band in samples C and D. In short, from samples A to D, the variation of electron wavefunction is less significant, whereas the hole wavefunction shows obvious movement to the left side of InGaN QWs, giving rise to the increase in overlap ratio of electron-hole wavefunctions. Thus, when the In gradient increases, the electron-hole wavefunction overlap becomes large, leading to an enhanced radiative recombination rate and an improved EL intensity from samples A to D.

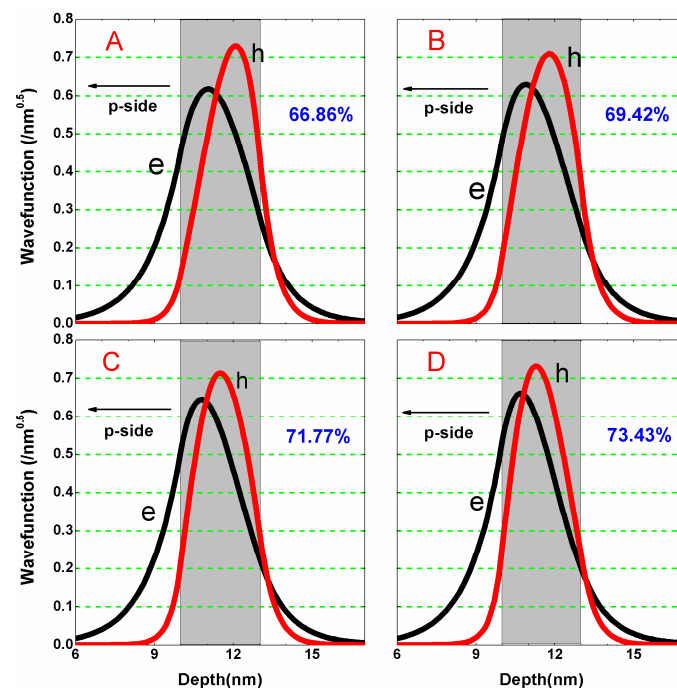


Figure 6. The wavefunctions of electrons (e) and holes (h) in the last QW for samples A, B, C and D.

#### 4. Conclusions

In summary, the effects of a linear increase in In content along the growth direction in InGaN QWs on the EL characteristics of 4 InGaN/AlGaIn UV MQWs with the same average In content are investigated numerically. It is found that as the In gradient increases, the samples' EL intensities are enhanced and the spectral peak wavelength increases, which may be ascribed to the different variations of conduction and valance bands influenced jointly by the polarization field and the gradually increased In content along the growth direction. As a consequence, the overlap of electron and hole wavefunctions increases, and more carriers concentrate on the left side of InGaIn layers, where the depth of potential well is the lowest in InGaIn QWs, leading to enhanced radiative recombination rate and spectral redshift, respectively.

**Author Contributions:** Conceptualization, J.Z. and W.L.; methodology, J.Z. and W.L.; software, J.Z.; validation, J.Z.; formal analysis, J.Z. and W.L.; resources, W.L.; data curation, J.Z.; writing—original draft preparation, J.Z.; writing—review and editing, J.Z. and W.L.; visualization, S.Z. All authors have read and agreed to the published version of the manuscript.

**Funding:** This research was funded by the National Natural Science Foundation of China, grant number 62074129.

**Institutional Review Board Statement:** Not applicable.

**Informed Consent Statement:** Not applicable.

**Data Availability Statement:** Data are available on request.

**Acknowledgments:** The authors would like to gratefully acknowledge the support from the National Natural Science Foundation of China.

**Conflicts of Interest:** The authors declare no conflict of interest. The funders had no role in the design of the study; in the collection, analyses, or interpretation of data; in the writing of the manuscript; or in the decision to publish the results.

#### References

1. Nakamura, S.; Mukai, T.; Senoh, M. Candela-Class High-Brightness InGaIn/AlGaIn Double-Heterostructure Blue-Light Emitting-Diodes. *Appl. Phys. Lett.* **1994**, *64*, 1687–1689.
2. Bae, S.; Kim, S.; Nam, E.S.; Lim, S.; Son, J.; Jo, Y. 380-nm Ultraviolet Light-Emitting Diodes with InGaIn/AlGaIn MQW Structure. *ETRI J.* **2013**, *35*, 566–570. [[CrossRef](#)]
3. Chen, P.; Park, Y.J.; Liu, Y.-S.; Detchprohm, T.; Yoder, P.D.; Shen, S.-C.; Dupuis, R.D. Epitaxial Growth and Optically Pumped Stimulated Emission in AlGaIn/InGaIn Ultraviolet Multi-Quantum-Well Structures. *J. Electron. Mater.* **2020**, *49*, 2326–2331. [[CrossRef](#)]
4. Li, Y.; Xing, Z.; Zheng, Y.; Tang, X.; Xie, W.; Chen, X.; Wang, W.; Li, G. High-efficiency near-UV light-emitting diodes on Si substrates with InGaIn/GaN/AlGaIn/GaN multiple quantum wells. *J. Mater. Chem. C* **2020**, *8*, 883–888. [[CrossRef](#)]
5. Mukai, T.; Morita, D.; Nakamura, S. High-power UV InGaIn/AlGaIn double-heterostructure LEDs. In Proceedings of the 2nd International Conference on Nitride Semiconductors (ICNS), Tokushima, Japan, 27–31 October 1997; pp. 778–781.
6. Kent, P.R.C.; Zunger, A. Carrier localization and the origin of luminescence in cubic InGaIn alloys. *Appl. Phys. Lett.* **2001**, *79*, 1977–1979. [[CrossRef](#)]
7. Lei, Y.; Liu, Z.; He, M.; Yi, X.; Wang, J.; Li, J.; Zheng, S.; Li, S.; Yan, L.; Zhiqiang, L.; et al. Enhancement of blue InGaIn light-emitting diodes by using AlGaIn increased composition-graded barriers. *J. Semicond.* **2015**, *36*, 54006. [[CrossRef](#)]
8. Chang, S.J.; Kuo, C.H.; Wu, L.W.; Sheu, J.K.; Wen, T.C.; Lai, W.C.; Chen, J.F.; Tsai, J.M. 400-nm InGaIn-GaN and InGaIn-AlGaIn multiquantum well light-emitting diodes. *IEEE J. Sel. Top. Quant.* **2002**, *8*, 744–748. [[CrossRef](#)]
9. Kim, K.; Kim, C.S.; Lee, J.Y. The In compositional gradation effect on photoluminescence in InGaIn/GaN multi-quantum-well structures. *J. Phys. Condens. Matter* **2006**, *18*, 3127–3140. [[CrossRef](#)]
10. Park, S.-H.; Moon, Y.-T.; Han, D.-S.; Park, J.S.; Oh, M.-S.; Ahn, D. Comparison of light emission in InGaIn/GaN light-emitting diodes with graded, triangular, and parabolic quantum-well structures. *J. Korean Phys. Soc.* **2012**, *60*, 505–508. [[CrossRef](#)]
11. Schubert, M.F.; Chhajed, S.; Kim, J.K.; Schubert, E.F.; Koleske, D.D.; Crawford, M.H.; Lee, S.R.; Fischer, A.J.; Thaler, G.; Banas, M.A. Effect of dislocation density on efficiency droop in GaInN/GaN light-emitting diodes. *Appl. Phys. Lett.* **2007**, *91*, 231114. [[CrossRef](#)]
12. Zhang, Z.-H.; Liu, W.; Ju, Z.; Tan, S.T.; Ji, Y.; Kyaw, Z.; Zhang, X.; Wang, L.; Sun, X.; Demir, H.V. Self-screening of the quantum confined Stark effect by the polarization induced bulk charges in the quantum barriers. *Appl. Phys. Lett.* **2014**, *104*, 243501. [[CrossRef](#)]



13. Cheng, L.-W.; Ma, J.; Cao, C.-R.; Xu, Z.-Z.; Lan, T.; Yang, J.-P.; Chen, H.-T.; Yu, H.-Y.; Wu, S.-D.; Yao, S.; et al. Improved carrier injection and confinement in InGaN light-emitting diodes containing GaN/AlGaIn/GaN triangular barriers. *Chin. Phys. B* **2018**, *27*, 088504. [\[CrossRef\]](#)
14. Soltani, M.; Jahromi, H.D.; Sheikhi, M.H. Highly Efficient AlGaIn/GaN/InGaIn Multi-quantum Well Ultraviolet Light-Emitting Diode. *Iran. J. Sci. Technol. Trans. Electr. Eng.* **2020**, *44*, 69–76. [\[CrossRef\]](#)
15. Zhou, S.; Xu, H.; Hu, H.; Gui, C.; Liu, S. High quality GaN buffer layer by isoelectronic doping and its application to 365 nm InGaIn/AlGaIn ultraviolet light-emitting diodes. *Appl. Surf. Sci.* **2019**, *471*, 231–238. [\[CrossRef\]](#)
16. Zhu, D.; Kappers, M.J.; Costa, P.M.F.J.; McAleese, C.; Rayment, F.D.G.; Chabrol, G.R.; Graham, D.M.; Dawson, P.; Thrush, E.J.; Mullins, J.T.; et al. A comparative study of near-UV emitting InGaIn quantum wells with AlGaIn and AlInGaIn barriers. In Proceedings of the International Conference on Nanoscale Magnetism (ICNM), Gebze, Turkey, 3–7 July 2005; pp. 1819–1823.
17. Yu, H.B.; Chen, Q.; Ren, Z.J.; Tian, M.; Long, S.B.; Dai, J.N.; Chen, C.Q.; Sun, H.D. Enhanced Performance of an AlGaIn-Based Deep-Ultraviolet LED Having Graded Quantum Well Structure. *IEEE Photonics. J.* **2019**, *11*, 8201006. [\[CrossRef\]](#)
18. Mishra, P.; Ng, T.K.; Janjua, B.; Shen, C.; Eid, J.; Alyamani, A.Y.; El-Desouki, M.M.; Ooi, B.S. Extending quantum efficiency roll-over threshold with compositionally graded InGaIn/GaN LED. In Proceedings of the 2014 IEEE Photonics Conference, San Diego, CA, USA, 12–16 October 2014; pp. 22–23.
19. Li, H.; Chang, C.J.; Kuo, S.Y.; Wu, H.C.; Huang, H.M.; Lu, T.C. Improved performance of near UV GaN-based light emitting diodes with asymmetric triangular multiple quantum wells. *IEEE J. Quant. Electron.* **2018**, *55*, 1–4. [\[CrossRef\]](#)
20. Shi, K.; Li, H.; Xu, M.; Li, C.; Wei, Y.; Xu, X.; Ji, Z. Photoluminescence properties of InGaIn/GaN multiple quantum wells containing a gradually changing amount of indium in each InGaIn well layer along the growth direction. *J. Lumin.* **2020**, *223*, 117225. [\[CrossRef\]](#)
21. Hao, R.; Chen, L.; Wu, J.; Fan, D.H.; Wu, Y.P.; Liang, S.H. Effects of growth temperature change in quantum well on luminescence performance and optical spectrum. *Optik* **2021**, *235*, 166606. [\[CrossRef\]](#)
22. Lee, Y.-J.; Chen, C.-H.; Lee, C.-J. Reduction in the Efficiency-Droop Effect of InGaIn Green Light-Emitting Diodes Using Graded Quantum Wells. *IEEE Photon. Technol. Lett.* **2010**, *22*, 1506–1508. [\[CrossRef\]](#)
23. Wang, L.; Li, R.; Yang, Z.W.; Li, D.; Yu, T.; Liu, N.Y.; Liu, L.; Chen, W.H.; Hu, X.D. High spontaneous emission rate asymmetrically graded 480 nm InGaIn/GaN quantum well light-emitting diodes. *Appl. Phys. Lett.* **2009**, *95*, 211104. [\[CrossRef\]](#)
24. Dong, H.L.; Jia, T.T.; Liang, J.; Zhang, A.Q.; Jia, Z.G.; Jia, W.; Liu, X.G.; Li, G.Q.; Wu, Y.C.; Xu, B.S. Improved carrier transport and photoelectric properties of InGaIn/GaN multiple quantum wells with wider well and narrower barrier. *Opt. Laser. Technol.* **2020**, *129*, 106309. [\[CrossRef\]](#)
25. Chung, H.Y.; Woo, K.Y.; Kim, S.J.; Kim, T.G. Improvement of blue InGaIn/GaN light-emitting diodes with graded indium composition wells and barriers. *Opt. Commun.* **2014**, *331*, 282–286. [\[CrossRef\]](#)
26. Fiorentini, V.; Bernardini, F.; Ambacher, O. Evidence for nonlinear macroscopic polarization in III-V nitride alloy hetero-structures. *Appl. Phys. Lett.* **2002**, *80*, 1204–1206. [\[CrossRef\]](#)
27. Karan, H.; Biswas, A.; Saha, M. Improved performance of InGaIn/GaN MQW LEDs with trapezoidal wells and gradually thinned barrier layers towards anode. *Opt. Commun.* **2017**, *400*, 89–95. [\[CrossRef\]](#)
28. Thomas, P.S.; Daniel, S.P.T.; Stefan, S. Atomistic analysis of piezoelectric potential fluctuations in zinc-blende InGaIn/GaN quantum wells: A Stillinger-Weber potential based analysis. *Phys. Rev. B* **2021**, *103*, 165201.
29. Hongtao, J.; Jasprit, S. Gain Characteristics of InGaIn–GaN Quantum Wells. *IEEE J. Quantum. Electron.* **2000**, *36*, 1058–1064. [\[CrossRef\]](#)